



Cite this: *Toxicol. Res.*, 2015, 4, 655

Uptake of gold nanoparticles in primary human endothelial cells†

Henrik Klingberg,^{a,b} Lene B. Oddershede,^b Katrin Loeschner,^c Erik H. Larsen,^c Steffen Loft^a and Peter Møller^{*a}

Gold nanoparticles (AuNPs) are relevant in nanomedicine for drug delivery in the vascular system, where endothelial cells are the first point of contact. We investigated the uptake of 80 nm AuNPs in primary human umbilical vein endothelial cells (HUVECs) by flow cytometry, 3D confocal microscopy, nano-scale 3D-imaging using focused ion beam/scanning electron microscopy (FIB/SEM), and single particle inductively coupled plasma-mass spectrometry (spICP-MS). HUVECs were cultured for 3 h or 24 h in medium with AuNPs in a concentration range of 1.25–10 $\mu\text{g ml}^{-1}$. There was a concentration-dependent increase of AuNPs inside cells measured by flow cytometry, spICP-MS and 3D confocal microscopy. The latter also showed that AuNPs were located in the cytosol. This was supported by FIB/SEM, showing that AuNPs were located in membrane enclosures in the cytoplasm as single particles or agglomerates of 2–3 or more particles. Pre-treatment with chlorpromazine inhibited the AuNP-uptake in HUVECs, indicating that internalisation occurred mainly by clathrin-mediated endocytosis. Cell activation by exposure to tumour necrosis factor or lipopolysaccharide had a slight or no effect on the uptake of AuNPs, respectively. The AuNP exposure did not influence cell cytotoxicity, whereas the intracellular reactive oxygen species production was slightly increased. In conclusion, the uptake of AuNPs by endothelial cells can be addressed quantitatively by several methods with high throughput and/or high specificity. Uptake of AuNPs in HUVECs occurred mainly by clathrin-mediated endocytosis and trafficking to membrane enclosures in the form of single particles and agglomerates of 2–3 particles.

Received 4th June 2014,
Accepted 6th August 2014

DOI: 10.1039/c4tx00061g

www.rsc.org/toxicology

Background

Gold nanoparticles (AuNPs) are considered to be candidates for the development of nanomedicine, for thermo-surgery due to their exceptional plasmonic properties,¹ and for DNA/RNA-delivery.^{2–6} In addition, they are widely used as model particles for particle–cell interaction studies.⁷ The plasmonic property of AuNPs cause their scattering and absorbance properties to be highly shape and size dependent.^{8,9} In addition, they can be manufactured with well-defined size, shape and surface chemistry.^{10–12}

The interaction between circulating NPs and vascular endothelial cells in blood vessels is important with regard to tissue delivery since the endothelium is the main barrier between

blood and tissues in animals.¹³ It has been shown that primary human dermal microvascular endothelial cells (HDMEC) and a human cerebral microvascular endothelial cell line (hCMEC/D3) possess the ability to take up AuNPs that were citrate-stabilised (\varnothing 10, 11 and 25 nm)¹⁴ or surface-modified with five different polymers (\varnothing 18, 35 and 65 nm).^{15,16} AuNPs modified for targeted delivery are also internalised as documented by the uptake of monocarboxy-(1-mercaptopentadec-11-yl) hexaethylene glycol (OEG) capped AuNPs (\varnothing 17 nm) with or without vascular endothelial growth factor type 1 receptor (VEGFR-1) and the neuropilin receptor (NRP-1) binding peptides.¹⁷ Primary human umbilical vein endothelial cells (HUVECs) have the ability to take up small positively or negatively charged AuNPs (\varnothing 5 nm),¹⁸ hollow core AuNPs (\varnothing 91 nm), Au shell/silica core AuNPs (\varnothing 43 nm) and Au-nanorods (17 × 47 nm, 2.8 : 1 aspect ratio).¹⁹

The most common uptake pathways for AuNPs are various forms of receptor-mediated endocytosis, including clathrin-, caveolin- or raft-dependent uptake.²⁰ Chlorpromazine (CPZ) and monodansyl cadaverine (MDC) are considered to be inhibitors of clathrin-mediated endocytosis,^{21,22} whereas nystatin is an inhibitor of clathrin-independent and cholesterol-dependent endocytosis.²³ On the other hand, uptake of NPs

^aDepartment of Public Health, Section of Environment Health, University of Copenhagen, Øster Farimagsgade 5B, DK-1014 Copenhagen, Denmark.

E-mail: pemo@sund.ku.dk

^bNiels Bohr Institute, University of Copenhagen, Blegdamsvej 17, DK-2100 Copenhagen, Denmark

^cDivision of Food Chemistry, National Food Institute, Technical University of Denmark, Mørkhøj Bygade 19, DK-2860 Søborg, Denmark

†Electronic supplementary information (ESI) available. See DOI: 10.1039/c4tx00061g

may also be promoted by stimulation of endothelial cells by inflammatory responses as shown for VCAM1-targeted uptake.²⁴

Here the cellular uptake of AuNPs was investigated with techniques that measure either the relative uptake compared to controls or the absolute uptake in mass concentration. The relative cellular AuNP-uptake can be obtained with a high throughput method based on label-free flow cytometry. In this technique, the forward-scattered light (FSC) and the side-scattered light (SSC) are measures of cell size and total cell reflection, respectively. This method takes advantage of the high scattering properties of Au (and other metallic) particles.²⁵ The magnitude of scattered light from spherical AuNPs with a diameter of 80 nm (at λ 560 nm) is 5 times greater than the magnitude of light emission of the commonly used intracellular dye calcein-AM (at λ 483 nm).²⁶ Flow cytometry and SSC detection have also been used to assess cellular silver-NP-uptake^{27,28} and TiO₂-NP-uptake.²⁹ In the present study, we also measured the relative AuNP-uptake quantitatively by 3D confocal laser scanning microscopy (CLSM), which is based on cell-staining and label-free detection of AuNPs by particle reflection, thereby avoiding possible bias from uneven distribution of particle-dye conjugation and bleaching of the fluorescence signal. Both flow cytometry and CLSM detect AuNP-uptake by reflection, but it is possible by CLSM image analysis to omit the intrinsic cellular reflection to obtain the signal only originating from the AuNPs.

To obtain the absolute quantification of cellular AuNP-uptake it is necessary to go beyond the diffraction limited optical systems. Inductively coupled plasma-mass spectrometry (ICP-MS) and inductively coupled plasma and atomic emission spectroscopy (ICP-AES) are standard methods for absolute quantification of cellular AuNP-uptake, whereas they provide little information regarding the particle size.^{5,30,31} Nevertheless, single particle ICP-MS (spICP-MS) has recently been developed to quantify the mass concentration of Au, particle size and particle number in tissue samples, although it can only be used for NPs with diameters larger than 20 nm.^{32,33}

Transmission electron microscopy (TEM) is highly relevant for studies on intracellular AuNP localisation.⁵ It is possible to visualise AuNPs directly using TEM because of the high resolution of the method (\sim 0.2 nm). The electron dense Au-atoms result in a high contrast between AuNPs and the biological matrix.³⁴ However, cell samples need to be fixed and manually sliced by a microtome for conventional TEM, which might cause sample artefacts due to the hardness of the particles as for instance shown for TiO₂.³⁵ Focused ion beam/scanning electron microscopy (FIB/SEM) makes it possible for matrix-embedded cells to be continuously sectioned by an ion beam (down to 10 nm per section) and images are subsequently assembled to a 3D SEM image.³⁶ The uptake of spherical AuNPs (3, 12 and 30 nm) in a human monocyte cell-line (THP-1) has previously been examined by FIB/SEM, but this did not focus on the 3D localisation of the AuNPs.³⁷

The purpose of our study was to measure the extent of cellular AuNP-uptake as well as the intracellular distribution and

agglomeration/aggregation in HUVECs. A large review recently summarised the studies on AuNP-uptake in mammalian cells, demonstrating that a substantial number of studies have shown the uptake of especially functionalised AuNPs with TEM, ICP-MS and ICP-AES techniques.²⁰ In the present study we have used primary human endothelial cells and the uptake of unlabelled non-functionalised AuNPs was assessed with 4 different methods, of which spICP-MS and 3D-localisation of single particles by FIB/SEM are novel with respect to cellular AuNP-uptake. AuNPs were used because they have well-defined particle size, can be measured by methods with either relative or absolute quantification, and are suitable as nanomedicine model NPs due to their optical properties and surface chemistry.

Methods

Cell culture

HUVECs (cat. # C-015-5C, lot # 887799, Gibco, NY, USA) were used between passage 2 and 7 and cultured in Endothelial Cell Growth Medium with Growth Supplement (Cell Applications Inc., San Diego, CA, USA) at 37 °C, 5% CO₂ and 95% humidity. This HUVEC medium contained 2% serum unless otherwise indicated. The cell-culture surfaces were coated with Embryo-Max® 0.1% Gelatin Solution (Merck Millipore, Darmstadt, Germany) for 30 min prior to cell seeding.

In some experiments endocytosis was inhibited by pre-treatment of the HUVECs for 30 min with CPZ (42.2 μ M, Sigma-Aldrich, St Louis, MO, USA), MDC (300 μ M, Sigma-Aldrich) or nystatin (20 μ M, Sigma-Aldrich). In other experiments HUVECs were exposed to tumour necrosis factor (TNF) (100 ng ml⁻¹, Sigma-Aldrich) or lipopolysaccharides (LPS) (100 ng ml⁻¹, Sigma-Aldrich) for 24 h to mimic an activation of the cells by an inflammatory response.

Hydrodynamic nanoparticle size characterisation

Hydrodynamic size-distribution of the AuNPs was analysed using NanoSight LM20 and video analysis software NanoSight Nanoparticle Tracking Analysis version 2.2 (NanoSight Limited, Salisbury, UK). Size-determination was done after 0, 5 and 25 h of incubation with or without HUVECs in HUVEC medium.

AuNP-exposure

Colloidal citrate-stabilised spherical AuNPs (\varnothing 80 nm) (BBI Solutions, Cardiff, UK) were centrifuged (2×10^3g) for 5 min, the supernatant was removed and the AuNPs were re-suspended in HUVEC medium by vortexing and diluted to 1.25–50 μ g ml⁻¹ (corresponding to 6–254 μ M and 2.42×10^8 – 9.67×10^9 particles per ml under all experimental conditions).

The sedimentation of AuNPs was assessed in cell-free Ibidi VI^{0.4} (Ibidi Treat) chambers (with or without gelatin 0.1% pre-coating), consisting of cell growth (volume height 0.4 mm and area 0.6 cm²) supported with cell culture media from two reservoirs (volume 120 μ l). The medium is applied in the reservoirs and subsequently flow to the growth area by capillary forces.

HUVEC medium containing $5 \mu\text{g ml}^{-1}$ AuNPs was added to the chambers and sealed to avoid evaporation. These were placed on a pre-heated (37°C) microscope stage and inspected for sedimentation after 24 h of incubation.

Flow cytometry

Samples were analysed on a BD Accuri™ C6 Flow Cytometer (Becton, Dickinson and Company, Franklin Lakes, NJ, USA). HUVECs were seeded (1×10^5 per well) on to Nunc™ 12 well plates (Nunc-Thermo Fisher Scientific, Roskilde, Denmark) one day prior to AuNP-exposure. AuNP-exposure (0, 1.25, 5 or $10 \mu\text{g ml}^{-1}$; 3 h) was ended by washing ($3\times$) in HEPES buffered saline solution (Lonza, Walkersville, MD, USA) followed by 1–2 min of incubation with 0.05% trypsin-EDTA (Gibco). Trypsinisation was terminated by addition of cold HUVEC medium, and samples were kept on ice until analysis by flow cytometry. A gate that included the entire cell population was established and 2×10^4 events were recorded within this gate (on fast collection to avoid sedimentation of large cells).

Confocal microscopy and 3D image analysis

Images were collected on a Leica SP5 confocal microscope using a Leica PL APO NA 1.2 $63\times$ water immersion objective (Leica Microsystems, Mannheim, Germany). A detailed description of the image acquisition can be found in the ESI.† Two days prior to AuNP-exposure, HUVECs were seeded (1.65×10^4 cells per channel) in 6-channeled Ibidi chambers (μ -Slide VI^{0.4}, IbiTreat, Ibidi, Planegg, Germany) and the HUVEC medium was replaced daily. After AuNP-exposure (0, 1.25, 2.5, 5 or $10 \mu\text{g ml}^{-1}$; 3 h and 24 h) HUVECs were stained with either Vybrant® DiI staining (1 min, 1:400 in 300 mM sucrose) or CellTracker™ Green 5-chloromethylfluorescein diacetate (CMFDA) staining (5 min, 20 μM in serum-free medium) (Molecular Probes®, Eugene, OR, USA) with washing procedures described by the manufacturer. HUVECs were fixed with 4% paraformaldehyde in PBS (Alfa Aesar, Ward Hill, MA, USA) for 30 min at room temperature and mounted in mounting medium (Ibidi). The staining of cells with CellTracker Green CMFDA has been shown to increase membrane stiffness.³⁸ Consequently, the cellular AuNP uptake was examined in HUVECs stained immediately before fixation in 4% paraformaldehyde. Subsequent 3D image processing and analysis was done using the Volocity® 3D Image Analysis Software (v.6.1.1., Perkin Elmer, Waltham, MA, USA). The 3D volumes of the CellTracker Green signal (cell volume) and AuNP reflection signal (AuNP volume) were measured and the AuNP volumes overlapping with the CellTracker Green volumes were used as a measure of internalised AuNPs. The volume of the AuNPs was only relatively compared with an absolute volume estimate because the signal size originating from a single particle does not represent the actual size of the particle, which is well below the diffraction limit of light ($\sim 200 \text{ nm}$).³⁸ The ratio between cell volume and AuNP volume was used as a measure of AuNP-uptake. The data were standardised according to the uptake in cells that were exposed to $1.25 \mu\text{g ml}^{-1}$ in each experiment. We did not standardise with respect to the control since there was no background AuNP-signal.

Sedimentation of the AuNPs under cell-free conditions was examined by confocal imaging (z-stacks) after 24 h of incubation (AuNPs were imaged as for cellular exposure experiments). AuNPs were detected by counting the number per area without size information.

Focused ion beam scanning electron microscopy (FIB/SEM)

Specimen milling and imaging was accomplished using a FEI Quanta FEG 3D (FEI Company, Hillsboro, OR, USA) equipped with a gallium ion-beam. The slice thickness was 20 nm and images were acquired at $50\,000\times$ magnification. 3D-reconstruction was done in Amira® (v.5.5.0, Visualization Sciences Group, Bordeaux, France). One day prior to AuNP exposure ($5 \mu\text{g ml}^{-1}$ for 24 h), 6.6×10^4 HUVECs were seeded on a $\varnothing 13 \text{ mm}$ Nunc™ Thermanox™ Coverslip (Thermo Fisher Scientific Inc., Rochester, NY, USA) placed in Nunc™ 12 well plates (Nunc-Thermo Fisher Scientific). Further detailed descriptions of EM-specimen preparation, FIB/SEM procedure and image reconstruction can be found in the ESI.†

Single particle inductively coupled plasma mass spectrometry (spICP-MS)

A Thermo Scientific iCAP Q ICP-MS instrument (Thermo Fisher Scientific, Bremen, Germany) was used for all spICP-MS experiments. Instrument tuning was performed prior to analysis by using a tuning solution according to the manufacturer's recommendations. Instrument settings are given in Table S1 of the ESI.† For each sample the ¹⁹⁷Au signal intensity was recorded for 180 s with a dwell time of 10 ms. Following the analysis of each sample, ultrapure water was analysed to ascertain that no carry-over from the previous measurement could be detected. The AuNP size distribution and measurements were modified from the experiments described previously.³² A detailed description of the method can be found in the ESI.†

HUVECs were set up and exposed as for CLSM with an exposure time of 24 h and 0, 1.25, 5 or $10 \mu\text{g ml}^{-1}$ AuNPs. The cells were thoroughly washed after the exposure period, followed by 1–2 min of trypsinisation with 0.5% trypsin EDTA (Gibco) and re-suspended in HUVEC medium. The cell number was obtained using Casy Model TT (Roche Diagnostics, Basel, Switzerland) and cells were frozen for analysis by spICP-MS. One day before spICP-MS, samples were thawed and diluted in BSA (Sigma Aldrich) in a concentration calculated to match adsorption by the expected AuNP concentration (see ESI†) to avoid particle agglomeration. Samples were treated with tetramethylammonium hydroxide (TMAH) (Alfa Aesar) for alkaline digestion in a final concentration of 5% (v/v). The samples were rotated mechanically at room temperature overnight. Before spICP-MS analysis the samples were diluted in ultrapure water to match an average particle count per sample of ~ 1000 – 5000 AuNPs.

Reactive oxygen species (ROS) generation and cell cytotoxicity

A multi-well fluorometer (Fluoroskan Ascent FC, Thermo Fischer Scientific) was used for 2',7'-dichlorofluorescein (DCFH, Sigma Aldrich) and calcein-AM (Molecular Probes)

fluorescence measurements as the assay for intercellular production of reactive oxygen species (ROS). A multi-well spectrophotometer (Multiskan FC, Thermo Fischer Scientific) was used to measure the formation of formazan from metabolised tetrazolium salt WST-1 (Roche Diagnostic GmbH, Mannheim, Germany) by cellular mitochondrial dehydrogenases. One day prior to AuNP-exposure, HUVECs were seeded (2×10^4 cells per well) on to 96-well plates (DCFH/calcein: black plates, Nunc A/S; WST-1: transparent plates, TPP, Trasadingen, Switzerland). HUVECs were exposed to AuNPs in 200 μ l HUVEC medium (0, 1.25, 5 or 10 μ g ml^{-1} ; 3 h and 24 h) for DCFH/calcein experiments. After AuNP-exposure, wells were aspirated and DCFH (30 μ M) and calcein-AM (0.5 μ M) in Hank's balanced salt solution (Sigma Aldrich) was incubated for 30 min. The supernatant was aspirated and cells were incubated for 3 h under standard cell culture conditions and the fluorescent signal was measured at λ 538 nm (excited at λ 485 nm) and background fluorescence at λ 602 nm (excited at λ 519 nm). HUVECs were exposed to AuNPs in 200 μ l HUVEC medium (0, 1 and 50 μ g ml^{-1} ; 24 h) for WST-1 experiments. Wells were aspirated and washed in Hank's medium followed by incubation of the WST-1 reagent for 2 h under standard cell culture conditions. By the manufacturer's instructions, plates were shaken and absorbance was measured at λ 450 nm and reference absorbance was measured at λ 630 nm.

Statistics

Statistical significance was assessed by linear regression analysis and ANOVA tests. The $P < 0.05$ level was accepted as the statistical significance level. The statistical analyses were performed using Statistica version 5.5 (StatSoft Inc., Tulsa, OK, USA).

Results

Particle characterisation

The AuNPs were declared to be spherical and citrate stabilised with a diameter of 80 nm (coefficient of variation <8%) by the manufacturer. We determined the hydrodynamic size-distribution by NanoSight (Brownian motion) analysis (Table 1). In serum-containing medium (2.5% serum) the size distribution was unimodal with a mean particle size and size-distribution mode of 122–129 and 94–116 nm, respectively, corresponding to single particles of around 80 nm with a possible protein corona. No obvious change in the medium colour was observed upon visual inspection.

Table 1 Hydrodynamic particle size of Au nanoparticles in serum-containing media. Nanosight video analysis of Brownian motions was used for size determination of Au nanoparticles suspended in HUVEC medium with 2% serum at various time-points. The results represent the mean and SD from 4 independent experiments

Time (h)	0	5	25
Mean size (nm)	122 \pm 4.7	128 \pm 6.2	129 \pm 3.9
Mode (nm)	94 \pm 2.5	112 \pm 2.4	116 \pm 5.7

The sedimentation of AuNPs was investigated over a 24 h period. The fraction of AuNP-sedimentation was estimated using particle detection counts (not taking relative particle sizes into account). The expected number of particles per growth area in each Ibidi chamber was calculated from the confocal image area and compared with total exposure (160 μ l, growth area and reservoirs) or growth area volume (26 μ l). The sedimentation after 24 h was 0.3% (SD = 0.2) or 1.7% (SD = 1.1) for total exposure and growth area volume, respectively. Ibidi chambers not coated with 0.1% gelatin had 2.7 fold (SD = 1.2) fewer particle counts as compared to coated samples.

Measurement of AuNP-uptake by flow cytometry

HUVECs were exposed to 1.25–10 μ g ml^{-1} of AuNPs for 3 h (Fig. 1). The cell granularity (SSC-A) was increased at 1.25 (1.17-fold, $P < 0.01$), 5 (1.43-fold, $P < 0.001$) and 10 μ g ml^{-1} (1.64-fold, $P < 0.001$) compared to unexposed cells, whereas there was no change in cell size (FSC-A) between exposed and unexposed cells (Fig. 1). The same gating scheme was used for all experiments (an example of an FSC-A/SSC-A gating plot and the raw data are available in the ESI Fig. S1†).

HUVECs were incubated with inhibitors of receptor-mediated endocytosis in order to investigate AuNP-uptake pathways. In addition, the HUVECs were activated with LPS or TNF pre-treatment in order to explore a possible increased cellular uptake of AuNPs. The cells were exposed to 5 μ g ml^{-1} of AuNPs for 3 h after the pre-treatment with endocytosis inhibitors or HUVEC-activating compounds (Fig. 1D). Clathrin-mediated endocytosis of AuNPs was inhibited by pre-treatment with CPZ (SSC-A: 0.9-fold change of the median unmodulated control, $P < 0.001$). Similar results on AuNP-uptake were obtained by pre-treatment with MDC, although this was only of borderline statistical significance (SSC-A: 1.18-fold, $P = 0.08$). Unexposed HUVECs modulated with CPZ and MDC had reduced SSC-A (CPZ: 0.79-fold, $P < 0.001$; MDC: 0.86-fold, $P < 0.001$). Caveolae-mediated endocytosis (lipid domain-mediated endocytosis) of AuNPs was not inhibited by pre-treatment with nystatin; no change in SSC-A in unexposed cells was observed. There was slightly increased SSC-A in HUVECs after modulation with LPS (1.13-fold, $P < 0.05$) or TNF (1.16-fold, $P < 0.05$). However, there was no difference in SSC-A between HUVECs that were exposed only to AuNPs (1.43-fold, $P < 0.05$) as compared to cultures that were pre-exposed to LPS (1.63-fold, $P < 0.05$) or TNF (1.43-fold, $P < 0.05$). The AuNP-uptake was slightly reduced in HUVECs that were pre-treated with TNF ($P < 0.05$, interaction between TNF and AuNP exposure). No change in SSC-A was observed in methanol controls (with respect to concentrations used for MDC samples). Unexposed HUVECs modulated with CPZ had a slightly reduced FSC-A (0.91-fold, $P < 0.02$), while no change was observed after modulation with MDC and nystatin compared to un-modulated cells (see SSC-A/FSC-A scatter plot in ESI Fig. S2†). TNF and LPS modulation slightly increased FSC-A (TNF: 1.15-fold, $P < 0.001$; LPS: 1.08-fold, $P < 0.05$). No change in FSC-A was observed after modulation with nystatin and methanol.

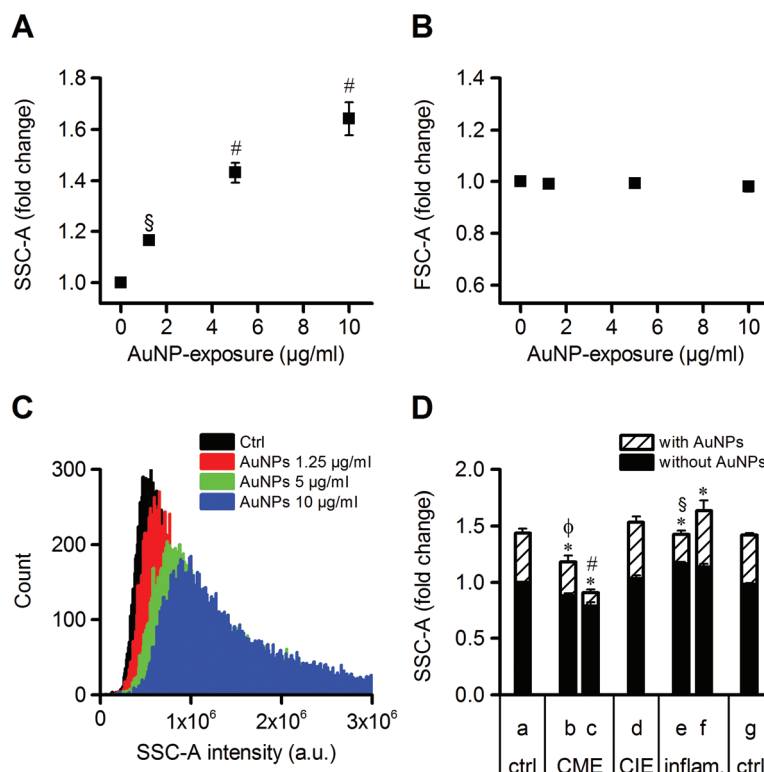


Fig. 1 Flow-cytometric analysis of HUVECs after 3 h of AuNP-exposure. Panel A shows the averaged median SSC-A (granularity) of cells exposed to AuNPs (0, 1.25, 5 or 10 $\mu\text{g ml}^{-1}$) relative to the unexposed control. $^{\S}P < 0.01$; $^{\#}P < 0.001$ compared to the unexposed control. Panel B shows the averaged median FSC-A (cell-size) of cells exposed to AuNPs (as for SSC-A) relative to the unexposed control. The results are fold difference (and SEM) compared to the control in 7 independent experiments. Panel C shows an overlay histogram of representative raw data from a single flow cytometry experiment exposed to AuNPs; each histogram represents 20 000 counts. Panel D shows the averaged median SSC-A for cells exposed to 5 $\mu\text{g ml}^{-1}$ AuNPs (hatched bars) or unexposed cells (black bar). These are overlaid into unmodulated control (a) or pre- and co-modulated samples: MDC (b), CPZ (c), nystatin (d), TNF (e), LPS (f) or methanol (g). These are grouped into controls (ctrl), clathrin-mediated endocytosis (CME), clathrin-independent endocytosis (CIE) or inflammatory activation (inflam.). $^*P < 0.001$ for the single-factor effect of Au or modulator. $^{\#}P < 0.001$, $^{\S}P < 0.05$, $^{\phi}P = 0.08$ for the interaction between Au and modulator. The results are fold difference (and SEM) compared to the unmodulated control in 3 (methanol), 5 (nystatin), 6 (TNF, LPS) or 7 (MDC, CPZ) independent experiments.

Measurement of AuNP-uptake by confocal microscopy

The level of AuNP-uptake and cellular localisation was investigated by CLSM with subsequent 3D-image analysis. HUVECs were exposed for either 3 h or 24 h with different concentrations of AuNPs (1.25–10 $\mu\text{g ml}^{-1}$) or for 3 h (5 $\mu\text{g ml}^{-1}$) for CPZ pre-treated cells. AuNPs were visualised in reflection-mode and HUVECs were stained with the fluorescent dye CellTracker Green CMFDA. Additional experiments with the membrane stain DiI (instead of CellTracker Green) were also conducted for the concentration titration experiments. An example of a 3D image of HUVECs after exposure to 5 $\mu\text{g ml}^{-1}$ of AuNPs is available as ESI S1.† The membrane-staining experiments showed that AuNPs were predominantly located within the cell, and only a few AuNPs located near or on the cell membrane (Fig. S3 in the ESI†). AuNPs were mostly present in the rounded perinuclear parts of the cell-body and to a lesser degree in the thinner periphery of the cell (Fig. 2). CellTracker Green CMFDA binds to intracellular thiol groups.^{39,40} The images do not contain specific staining of the nucleus, but the high concentration of CellTracker and the short incubation

time before fixation make it possible to distinguish certain stained membrane-enclosed regions in the cytosol. The nucleus appeared to have no content of AuNPs, while AuNPs appeared to localise in regions with lower CellTracker fluorescence intensity, indicating that the AuNPs were located in endosomes and lysosomes that were less stained with CellTracker with our experimental protocol (see movie file S2 and Fig. S3, panel A, in the ESI†). However, there were also AuNPs at locations with high CellTracker fluorescence intensity, ruling out the possible quenching of the fluorescence signal by AuNPs. Some intracellular agglomeration of AuNPs was observed, especially in the cells that had been exposed to the highest concentration of AuNPs (see Fig. 2C).

The volumes of both cells and internalised AuNPs were quantified in order to assess the cellular AuNP-uptake in HUVECs that had been exposed to particles for either 3 h or 24 h. After 3 h of AuNP-exposure, an increased AuNP/cell-volume ratio was found with increasing exposure concentrations in a linear manner (Fig. 2D, $r = 0.88$, $P < 0.001$). There was statistically significantly increased AuNP-uptake at 5 $\mu\text{g ml}^{-1}$ (2.78-fold, $P < 0.05$) and 10 $\mu\text{g ml}^{-1}$ (5.15-fold, $P < 0.001$)

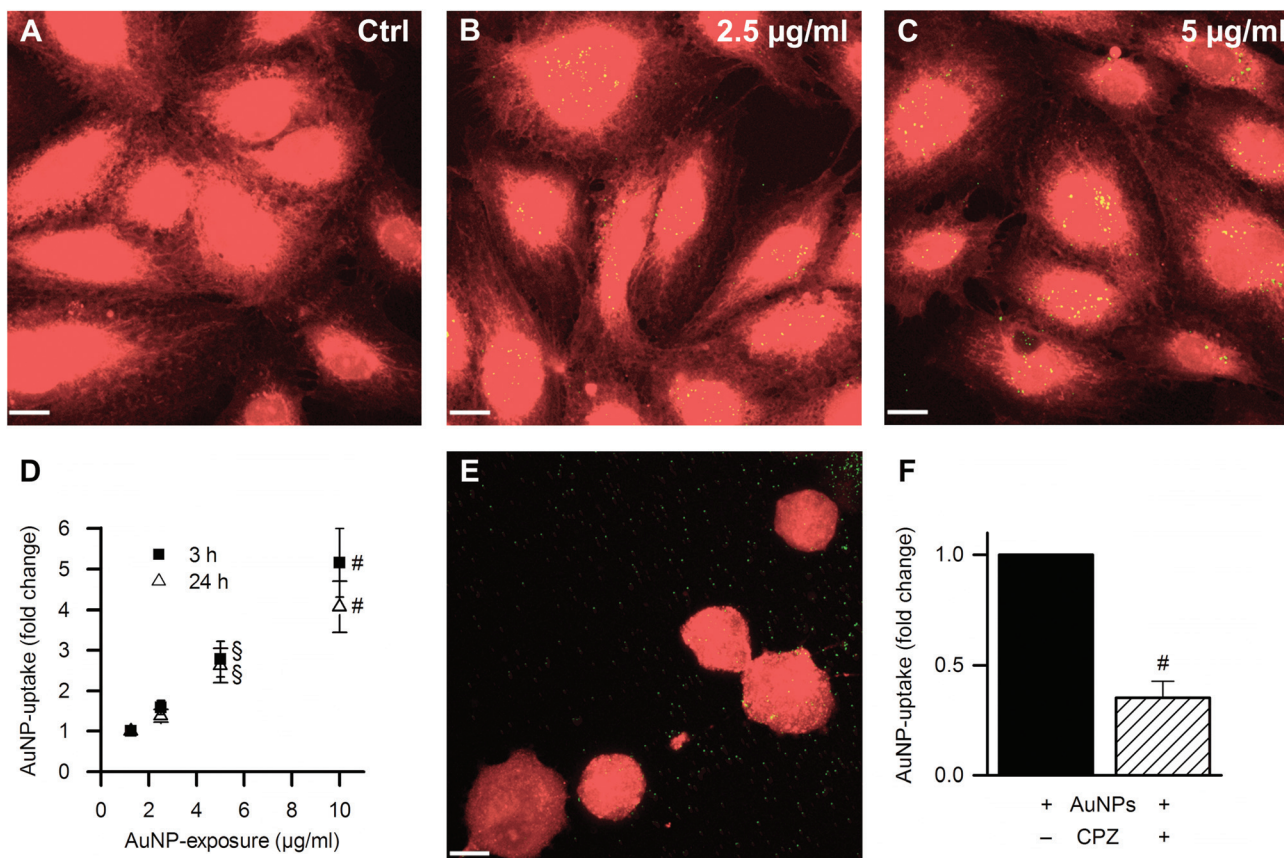


Fig. 2 Confocal microscopy analysis of HUVECs after 3 h and 24 h of AuNP-exposure. Panels A–C show HUVECs labelled with the cytosol stain CellTracker Green (red) and AuNPs (green/yellow) (scale bar = 15 µm). Panel D shows the quantified volume ratios between HUVECs and AuNPs after 3 h (■) and 24 h (△). The HUVECs were exposed to 0, 1.25, 2.5, 5 or 10 µg ml⁻¹. The results are fold changes (and SEM) compared to the 1.25 µg ml⁻¹ exposure group in the 3 and 24 h, separately. Panel E shows HUVECs pre-treated with CPZ and exposed with 5 µg ml⁻¹ AuNPs in the presence of CPZ for 3 h (scale bar = 19 µm). Panel F shows the quantified volume ratio between HUVECs and AuNPs after 3 h of exposure to 5 µg ml⁻¹ with or without CPZ. #*P* < 0.001, §*P* < 0.05; SEM for concentration titration experiments *n* = 4 and for CPZ experiments *n* = 5.

compared to 1.25 µg ml⁻¹. The 24 h AuNP-exposure period was also associated with increased AuNP-/cell-volume ratio (Fig. 2E, *r* = 0.87, *P* < 0.001). There was significantly increased AuNP-uptake at 5 µg ml⁻¹ (2.78-fold, *P* < 0.05) and 10 µg ml⁻¹ (4.08-fold, *P* < 0.001) compared to 1.25 µg ml⁻¹.

The pre-treatment with CPZ (42 µM) resulted in 65% (95% confidence interval: 45%–84%) reduced uptake of AuNPs as compared to controls (Fig. 2F, *P* < 0.001). Furthermore, most AuNPs in the CPZ pre-treated cells were located near or on the plasma membrane (see Fig. S4 in ESI†). Hence, it was not possible to distinguish internal or external localisation of AuNPs, leading to a possible overestimation of the uptake of AuNPs in CPZ pre-treated cells. Furthermore, the pre-treatment with CPZ changed somewhat the morphology of the HUVECs with reduced adherence area to the slides and rounded shapes (Fig. 2E) as compared with the flat cobblestone morphology of endothelial cells (Fig. 2A–C).

The fraction of AuNP-uptake was also assessed by particle detection counting, with the same procedure utilised for the AuNP-sedimentation experiments. The expected number of particles per growth area was calculated from the confocal

image area and compared with the total exposure volume (including reservoir). Cells exposed to 5 µg ml⁻¹ AuNPs for 24 h had an uptake of 1.5% (SD = 0.2) or 9.0% (SD = 1.1) of the total AuNPs in the total exposure volume (160 µl) or growth area (26 µl), respectively.

Measurement of AuNP-uptake by spICP-MS

Quantification of AuNP-uptake by spICP-MS showed a concentration-dependent relationship between the exposure concentration and cellular uptake/association (Fig. 3A). HUVECs were seeded as for CLSM analysis and exposed to AuNPs (1.25–10 µg ml⁻¹) for 24 h. There was an increased number of AuNPs per cell at both 5 µg ml⁻¹ (262-fold, *P* < 0.001) and 10 µg ml⁻¹ (333-fold, *P* < 0.001) compared to unexposed cells. We used unexposed HUVECs, spiked with AuNPs (spiked sample), and cell-free AuNP suspension (in water) to demonstrate that the median size of AuNPs in the assay was 80 nm (Fig. 3B). The detected particle size in AuNP-exposed HUVECs was similar to the declared diameter of 80 nm from the manufacturer (Fig. 3C). Agglomeration of the AuNPs could not be detected since no secondary peaks were observed as

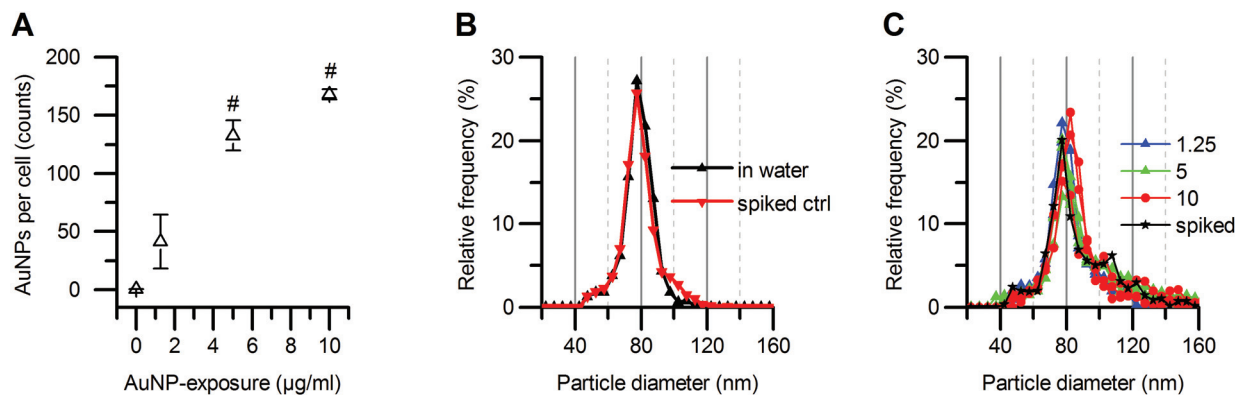


Fig. 3 spICP-MS analysis of HUVECs after 24 h of AuNP-exposure. Panel A shows the quantified particle count after exposure to 0, 1.25, 5 or 10 $\mu\text{g ml}^{-1}$. Panel B shows the relative frequency of size-distribution of AuNPs either in water or in unexposed control (spiked ctrl) both treated in tetramethylammonium hydroxide. Panel C shows the obtained size-distribution of AuNPs in HUVECs after exposure to AuNPs, including a spiked non-exposed control (spiked). $^{\#}P < 0.001$ compared to unexposed control; SEM for 5 and 10 $\mu\text{g ml}^{-1}$ $n = 3$ and for 0 and 1.25 $\mu\text{g ml}^{-1}$ $n = 2$.

compared to the AuNP-only control (this is also observed for the spiked control). However, it cannot be excluded that sample preparation (TMAH treatment and high sample dilution) led to disagglomeration of AuNPs, which had agglomerated in the cell culture.

Focused ion-beam scanning electron microscopy (FIB/SEM)

By inspecting the FIB/SEM 3D-images, AuNPs were observed in cytoplasmic membrane enclosures in HUVECs, most likely endosomes and liposomes (Fig. 4). HUVECs were exposed to 5 $\mu\text{g ml}^{-1}$ AuNPs for 24 h. Videos of the aligned raw image stack (ESI S3[†]) and rendered 3D image (ESI S4[†]) can be found in the ESI.[†] There were no AuNPs attached to the cell-surface, in mitochondria or in the nucleus. The AuNPs were located as agglomerates of varying sizes from 2–3 AuNPs per agglomerate

to larger clusters. In the 3D image the AuNPs appeared elongated in the z-plane, which might be caused by the back-scatter of electrons with varying penetration depth. The internalised AuNPs had a measured diameter of 120 nm, which was larger than the 80 nm measured by other techniques. This could be related to an angled electron back-scatter from the spherical AuNPs, causing spreading of electrons and blurring in the final image.

ROS production and cytotoxicity after exposure to AuNPs

The intracellular ROS production was measured after 3 and 24 h of exposure to AuNPs (1.25–10 $\mu\text{g ml}^{-1}$) with the use of the intracellular ROS-sensitive fluorescent probe DCFH (Fig. 5A). There was increased ROS production in HUVECs after 24 h of exposure to 5 $\mu\text{g ml}^{-1}$ ($P < 0.05$) and 10 $\mu\text{g ml}^{-1}$

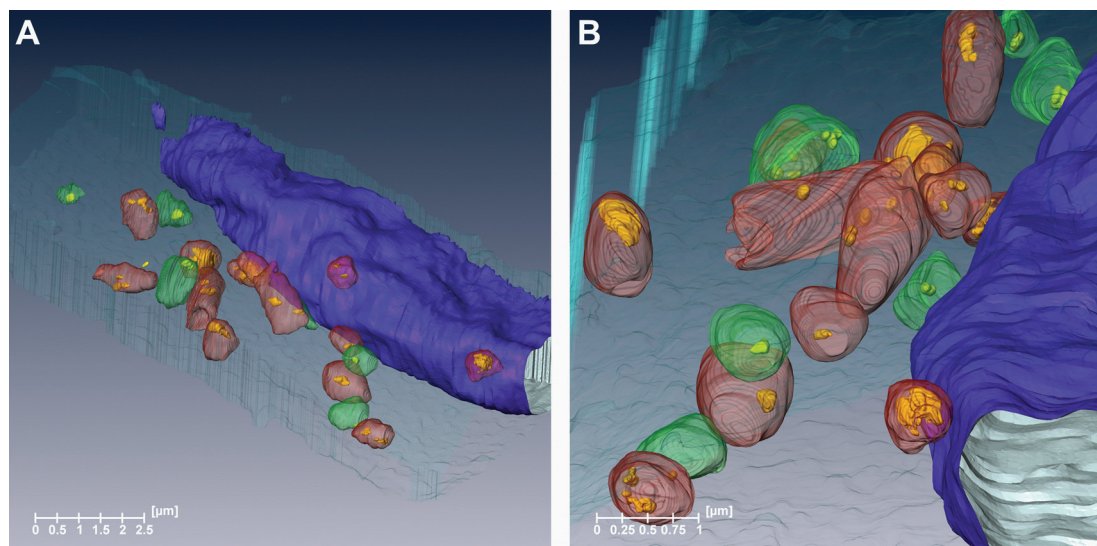


Fig. 4 FIB/SEM images of HUVECs after 24 h of exposure to 5 $\mu\text{g ml}^{-1}$ AuNPs. Panels A and B show HUVECs from two different viewing angles. The transparent magenta is the cell perimeter, the non-transparent blue is the nucleus, the transparent green is endosomes (low stained cytoplasmic membrane enclosures), the transparent red is lysosomes (highly stained cytoplasmic membrane enclosures), and the non-transparent yellow is AuNPs.

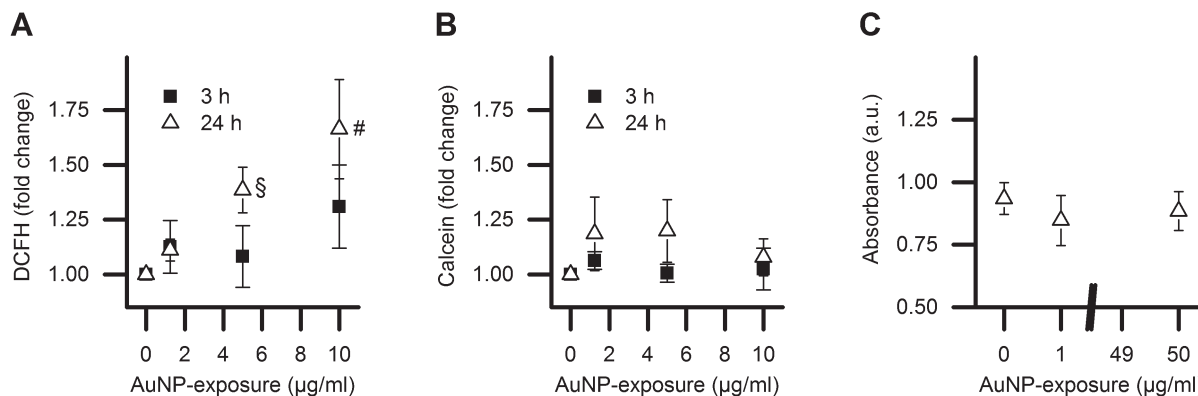


Fig. 5 Reactive oxygen species (ROS) production and cytotoxicity assessment of HUVECs exposed to AuNPs. Panel A shows the ROS production as fold change in DCFH signal compared to unexposed controls after 3 h and 24 h of exposure to AuNPs (1.25, 5, and 10 $\mu\text{g ml}^{-1}$). Panel B shows calcein-AM cell staining. Panel C shows the mitochondrial dehydrogenase activity as WST-1 signal after 24 h of exposure to AuNPs (0, 1 and 50 $\mu\text{g ml}^{-1}$). # $P < 0.01$, § $P < 0.05$; SEM for DCFH, $n = 5$, and for WST-1, $n = 3$.

($P < 0.01$) of AuNPs as compared to the non-exposed control. The 3 h exposure period was not associated with increased ROS production.

The number of cells was unaltered after 3 and 24 h of exposure to AuNPs as indicated by the intracellular stain calcein-AM (Fig. 5B). In addition, the WST-1 formation was also unaffected in HUVECs after 24 h of exposure to AuNPs (1 and 50 $\mu\text{g ml}^{-1}$) (Fig. 5C).

Discussion

The results from flow cytometry, 3D CLSM-image analysis and spICP-MS showed a concentration-dependent relationship between the exposure and cellular AuNP-uptake in HUVECs. The AuNP-uptake was substantially inhibited by pre-treatment with CPZ as shown by both flow cytometry and CLSM. CPZ and MDC are considered to be inhibitors of mainly clathrin-mediated endocytosis.^{21,41} Up-regulation of compensatory clathrin-independent pinocytosis after inhibition of clathrin-mediated endocytosis has previously been described.⁴² This could explain the difference in AuNP internalisation observed for HUVECs modulated with CPZ and MDC since a possible compensatory non-clathrin mediated endocytosis pathway could be co-inhibited by effects of CPZ with respect to actin dynamics.⁴³ Furthermore, an alternative endocytosis pathway could also be affected by the increased plasma-membrane fluidity also associated with CPZ.⁴⁴ A possible alternative internalisation pathway could be the recently discovered flotillin-involved endocytosis which can be both clathrin- and caveolae-independent but associated with actin dynamics.⁴⁵ The flotillin-involved endocytosis pathway has been suggested for poly(2-hydroxypropylmethacrylamide)-coated AuNPs (\varnothing 35 nm), which was found to be localised in late endosomes and lysosomes associated with flotillin-1 (HDMEC) and flotillin-2 (hCMEC/D3) independently of clathrin- and caveolae-mediated endocytosis.¹⁶

The observations indicate that clathrin-mediated endocytosis is a possible pathway of unmodified citrate-stabilised AuNP-uptake in HUVECs, whereas the unaltered AuNP-uptake in nystatin pre-treated cells indicates that caveolae-dependent endocytosis has less importance in HUVECs for AuNP-uptake. On the other hand, activation of HUVECs by treatment with LPS had little effect on the uptake of AuNPs, whereas the TNF pre-treatment was associated with a slightly reduced AuNP internalisation. Internalisation of AuNPs is typically attributed to receptor-mediated endocytosis in cells lacking phagocytosis activity.²⁰ We used citrate-stabilised and surface unmodified AuNPs in these experiments, whereas other reports are based on surface-modified AuNPs. For instance, it has been shown that transferrin-coated AuNPs (\varnothing 50 nm) were transported by clathrin-mediated endocytosis in HeLa cells.⁴⁶ Another study showed that herceptin-coated AuNPs (\varnothing 40 nm) were internalised by receptor mediated endocytosis in human breast cancer (SK-BR-3) cells.⁴⁷ Collectively, the results show that surface-unmodified AuNPs are internalised by the same mechanism as AuNPs that have been surface-modified with peptides or proteins. Still, we incubated HUVECs with AuNPs in serum-containing medium, which could promote formation of a protein corona on AuNPs,⁴⁸ and thus facilitate endocytosis of surface unmodified AuNPs. Citrate stabilised AuNPs have been shown to have fast adsorption of albumin in serum.⁴⁹ This together with the increased hydrodynamic particle size in medium containing serum we observed supports the notion of a protein corona formation (Table 1).

The CLSM analysis showed that the AuNPs were located on the external side of the plasma membrane of the CPZ exposed HUVECs and that the cells had a rounded morphology, different from the normal cobblestone-like morphology observed in non-modulated HUVECs. This altered morphology may affect internalisation and intracellular localisation of AuNPs in the CPZ treated cells as compared to control cells. It has previously been observed that CPZ at high concentrations (150 μM) modulated the morphology of endothelial cells, which appeared to have rounded shapes and reduced

adherence areas to the slides in CLSM.⁵⁰ The altered cell morphology could be caused by CPZ-mediated arrest of actin polymerisation, although this may be a cell-specific effect. It has been shown that CPZ reduced viability in cell lines of fibroblasts (COS-7) and African green monkey kidney epithelial (Vero) cells, whereas human hepatocellular carcinoma (HuH-7), retinal pigment epithelial (ARPE-19 cells), and retinal pigment epithelial (D407) cells were relatively insensitive with regard to viability to the concentration used in our study.⁴¹ Although CPZ reduced viability in Vero cells was associated with increased SSC-A, we found only reduced SSC-A in HUVECs after exposure to CPZ. The exposure to CPZ slightly reduced the cell size (FSC-A), but we found no sign of apoptotic body formation by CLSM. Similarly, MDC has been found to reduce viability for some cell types (HuH-7 and Vero cells) at a concentration that was 33 times higher (10 mM) than the one used in the present study (300 μ M). Other cell types (COS-7, ARPE-19 and D407) have been unaffected by MDC exposure. Furthermore, D407 cells showed a rounded phenotype after 2 h of incubation with 3 mM MDC, but there was no effect on cell viability.⁴¹

It has previously been shown that the gravitational pull on AuNPs in suspension promoted the interaction with adherent cells, which was attenuated by culturing cells in an inverted fashion with the cells facing downwards in the exposure medium.⁵¹ Furthermore, Cohen *et al.* reported that some metal oxide NPs and AuNPs (20 nm) were delivered to the cell culture area within a 24 h period, whereas certain types of carbon-based and metal oxide NPs were delivered over a longer period of time.⁵² Nevertheless, these results are not directly comparable to our sedimentation data because of different experimental set-up (open wells *versus* Ibidi chambers) and detection techniques used. Cohen *et al.* used a delivery system based on the ability of NPs to diffuse through and sediment on a porous membrane (3 μ m), whereas we used CSLM images to assess the number of delivered particles. The NP delivery was based on an *In vitro* Sedimentation, Diffusion and Dosimetry (ISDD) computational model, which overestimated the cellular delivery of silica NPs (2–3-fold), and the sedimentation was assessed under acellular conditions using carboxylated polystyrene NPs and positively charged poly-L-lysine coated cell culture dishes.⁵³ We used Ibidi chambers with negatively charged cell growth area. The repulsive forces between the cell growth area and the negatively charged AuNPs could explain the low sedimentation rate in our experiment and difference in sedimentation/delivery between our data and those reported by Cohen *et al.*⁵⁴ Nevertheless, it should be emphasised that we observed five times higher delivery under cellular conditions as compared to acellular conditions, indicating that the sedimentation alone did not determine internalisation of AuNPs in HUVECs. This difference is underestimated since it represents “particle detection” counts without taking into account the increased agglomeration of NPs in the HUVECs.

Earlier studies have used increased SSC-A by flow cytometry for the measurement of uptake in cultured cells after exposure to AuNPs⁵⁵ as well as nanosized silver, iron oxide, and

TiO₂.^{56–58} We observed a concentration-dependent increase in the SSC-A of HUVECs after 3 h of exposure to AuNPs. Similar observations have been obtained in K562 leukaemia cells where the concentration of 18 nm AuNPs decreased in the cell culture medium during the 2–3 h of incubation and subsequently remained low in the medium, which coincided with intracellular presence of AuNPs.⁵⁹ In addition, there was only about 5% exocytosis of transferrin-coated 74 nm AuNPs in fibroblasts, whereas the extent of exocytosis increased with decreasing primary particle size.⁴⁶ In our study there was a similar slope of the concentration–response curve for AuNP-uptake at 3 and 24 h, although it should be emphasised that it is not an absolute determination of AuNP-uptake across exposure times because there is no internal standard and the uptake was normalised to the lowest concentration (1.25 μ g ml⁻¹) rather than the unexposed cells. In another study there was a higher level of uptake of surface modified AuNPs (\varnothing 18, 35 and 65 nm) after 24 h as compared with 3 h in endothelial cells.¹⁵

The analysis of AuNP-uptake by CLSM and FIB/SEM indicated that the particles were located in the cytosol rather than in the nucleus of the cells. The AuNPs appeared to cluster inside the cytosol, which could be due to agglomeration of the particles before internalisation or trafficking of AuNPs to the same compartments within the cells (secondary agglomeration). The clusters consisted of 2–3 AuNPs, which is a bit too large for clathrin-mediated endocytosis with an optimal capacity of endocytosis of particles less than 100 nm.⁶⁰ Collectively, this suggests that the clusters of AuNPs are formed by secondary agglomeration. The FIB/SEM analysis did not unequivocally reveal that the AuNPs were located in compartments encapsulated by membranes such as endosomes. The analysis by spICP-MS actually indicated that the AuNPs retained their pristine size within the cell, although it should be noted that the assay protocol for determination of AuNPs might be associated with breakage of subtle agglomeration of protein-coated AuNPs.

Four different techniques reveal that AuNPs are internalised by HUVECs in our experiments (Table 2 summarises the utility of these methods). The flow cytometry analysis has the obvious advantage of being suitable for high throughput assessment, which is desirable if a substantial number of nanomaterials are being investigated. For instance, this method can be utilised to investigate the uptake of NPs with different surface modifications or concentrations. However, the flow cytometry analysis offers no direct proof of uptake of NPs because it is based on the light scattering of the whole cell. In addition, ideally there should be the same baseline level of SSC-A and FSC-A in controls and cells pre-treated with compounds affecting uptake of NPs, but this may not be possible as for instance shown in our experiments on CPZ and MDC inhibition of internalisation of AuNPs. There are limitations with regard to the analysis of size and shape of internalised NPs because of the diffraction limit by flow cytometry. The 3D CLSM provides detailed information about the intracellular localisation of NPs. Although it is still a relative

Table 2 Methods for the determination of intracellular uptake of Au nanoparticles

Method	Quantification ^a	Particle size	Intracellular localization	Specificity ^b	Throughput ^c
Flow cytometry	Relative	No	No	No	High
Confocal microscopy (CLSM)	Relative	No	Yes	Yes (metallic/fluorescent particles)	Low
spICP-MS	Absolute	Yes (for NPs >20 nm)	No	Yes	Medium
FIB/SEM	No	Yes	Yes	Yes (particles with heavy atoms)	Low

^a Absolute quantification refers to assessment of differences in particle number or mass concentration, whereas relative quantification refers to differences in proxy-measures such as side scattering (flow cytometry) or fluorescence signal (microscopy). ^b The specificity refers to certainty of the detection being Au nanoparticles (e.g. chemical detection of Au is a stronger proof than visual inspection of images for dark spots resembling nanoparticles). ^c The categorisation of throughput is relative to other methods of detection of Au nanoparticle uptake.

measurement that is based on reflection detection, the diffraction limitation precludes visual differentiation between particles with different sizes and shapes in the nanosize range, and calibration with internal standards is not possible by conventional CLSM. In addition, CLSM offers the possibility of live imaging of endocytosis as for instance shown in cultured mouse lung endothelial cells that accumulated gold-labelled albumin over a 20 min period⁶¹ and the integration with other techniques, e.g., optical manipulation.

Traditional TEM imaging has indicated that AuNPs (30–65 nm) accumulated over a 3 h period, forming clusters of particles in the cytoplasm.^{62,63} The advantage of FIB/SEM is obvious as it produces a 3D image of the cell with a resolution that allows separation of single NPs and agglomerates, although data acquisition and quantification of uptake would be overwhelmingly laborious in the case of analysis of multiple cells. Our experimental system showed that AuNPs were located in membrane enclosures, possibly endosomes or lysosomes. In keeping with the earlier analysis by TEM, we observed that AuNPs were located as single particles, agglomerates of 2–3 particles or large clusters. This was further supported by spICP-MS, indicating that AuNPs within the cell were predominantly present as 80 nm particles, although this method does not provide information of intracellular localisation of AuNPs.

The exposure to AuNPs was not associated with cytotoxicity as determined by the WST-1 assay that measures mainly succinate dehydrogenase activity within the cell. This is in keeping with observations that citrate-stabilised AuNPs only affected viability at high concentration (1 mM).¹⁴ Negatively charged spherical AuNPs, similar to the ones that we have used, are generally considered to be non-toxic.⁶⁴ The unaltered FSC measured by flow cytometry in our study also indicated that cell size was not affected. There was a slightly increased intracellular production of ROS after 24 h of exposure to AuNPs, whereas a 3 h period did not increase the ROS production. This might be due to a slightly increased activity of endogenous ROS producing enzymes such as NADPH oxidase. In addition, this ROS production in HUVECs is substantially smaller than the production observed in the same cells after exposure to other NPs. For instance, nanosized carbon black causes 10-fold increased ROS production at 3 h of exposure, which also is associated with oxidative damage to DNA and

mutations in cultured lung epithelial cells as well as activation of HUVECs as evidenced by increased expression of VCAM1 on the cell surface.^{65–68} It is therefore likely that the slightly increased ROS production in the AuNP exposed HUVECs at 24 h is related to activation of the cells rather than sustained oxidative stress.

In conclusion, our results show that cellular uptake of AuNPs is proportional to the concentration of AuNPs in the media. The uptake by endothelial cells occurs mainly by clathrin-mediated endocytosis. Internalised AuNPs are located in membrane enclosures and mainly as agglomerates of 2–3 AuNPs. Our study demonstrates that a combination of methods, based on 3D imaging and absolute physicochemical analysis, provide complementary data describing both the extent of AuNP uptake and localisation and the size of internalised nanoparticles.

Acknowledgements

The study was supported by the Lundbeck Foundation Center for Biomembranes in Nanomedicine. We acknowledge the Core Facility for Integrated Microscopy, Faculty of Health and Medical Sciences, University of Copenhagen where SEM specimen preparation, FIB/SEM imaging, and Amira image analysis were conducted. The Perkin Elmer Volocity 3D image analysis was conducted at the Center for Advanced Bioimaging (CAB) Denmark, University of Copenhagen.

References

- 1 P. M. Bendix, S. N. Reihani and L. B. Oddershede, *ACS Nano*, 2010, **4**, 2256–2262.
- 2 E. Boisselier and D. Astruc, *Chem. Soc. Rev.*, 2009, **38**, 1759–1782.
- 3 D. A. Giljohann, D. S. Seferos, W. L. Daniel, M. D. Massich, P. C. Patel and C. A. Mirkin, *Angew. Chem., Int. Ed.*, 2010, **49**, 3280–3294.
- 4 A. S. Thakor, J. Jokerst, C. Zavaleta, T. F. Massoud and S. S. Gambhir, *Nano Lett.*, 2011, **11**, 4029–4036.
- 5 E. C. Dreaden, A. M. Alkilany, X. Huang, C. J. Murphy and M. A. El-Sayed, *Chem. Soc. Rev.*, 2012, **41**, 2740–2779.

- 6 P. Tiwari, K. Vig, V. Dennis and S. Singh, *Nanomaterials*, 2011, **1**, 31–63.
- 7 R. A. Sperling, P. Rivera Gil, F. Zhang, M. Zanella and W. J. Parak, *Chem. Soc. Rev.*, 2008, **37**, 1896–1908.
- 8 H. Ma, P. M. Bendix and L. B. Oddershede, *Nano Lett.*, 2012, **12**, 3954–3960.
- 9 H. Ma, P. Tian, J. Pello, P. M. Bendix and L. B. Oddershede, *Nano Lett.*, 2014, **14**, 612–619.
- 10 M. C. Daniel and D. Astruc, *Chem. Rev.*, 2004, **104**, 293–346.
- 11 H. Jans and Q. Huo, *Chem. Soc. Rev.*, 2012, **41**, 2849–2866.
- 12 K. L. Kelly, E. Coronado, L. L. Zhao and G. C. Schatz, *J. Phys. Chem. B*, 2003, **107**, 668–677.
- 13 W. C. Aird, in *Endothelial Biomedicine*, Cambridge University Press, New York, 2007, pp. 227–229.
- 14 C. Freese, C. Uboldi, M. I. Gibson, R. E. Unger, B. B. Weksler, I. A. Romero, P. O. Couraud and C. J. Kirkpatrick, *Part. Fibre Toxicol.*, 2012, **9**, 23.
- 15 C. Freese, M. I. Gibson, H. A. Klok, R. E. Unger and C. J. Kirkpatrick, *Biomacromolecules*, 2012, **13**, 1533–1543.
- 16 C. Freese, R. E. Unger, R. C. Deller, M. I. Gibson, C. Brochhausen, H. A. Klok and C. J. Kirkpatrick, *Biomater. Sci.*, 2013, **1**, 824.
- 17 D. Bartczak, T. Sanchez-Elsner, F. Louafi, T. M. Millar and A. G. Kanaras, *Small*, 2011, **7**, 388–394.
- 18 D. Huhn, K. Kantner, C. Geidel, S. Brandholt, I. De Cock, S. J. Soenen, P. Rivera Gil, J. M. Montenegro, K. Braeckmans, K. Mullen, G. U. Nienhaus, M. Klapper and W. J. Parak, *ACS Nano*, 2013, **7**, 3253–3263.
- 19 D. Bartczak, O. L. Muskens, S. Nitti, T. Sanchez-Elsner, T. M. Millar and A. G. Kanaras, *Small*, 2012, **8**, 122–130.
- 20 L. A. Dykman and N. G. Khlebtsov, *Chem. Rev.*, 2014, **114**, 1258–1288.
- 21 A. I. Ivanov, in *Exocytosis and Endocytosis*, ed. A. I. Ivanov, Humana Press, 2008, vol. 440, ch. 2, pp. 15–33.
- 22 D. Dutta and J. G. Donaldson, *Cell. Logist.*, 2012, **2**, 203–208.
- 23 K. G. Rothberg, J. E. Heuser, W. C. Donzell, Y. S. Ying, J. R. Glenney and R. G. Anderson, *Cell*, 1992, **68**, 673–682.
- 24 H. Yang, F. Zhao, Y. Li, M. Xu, L. Li, C. Wu, H. Miyoshi and Y. Liu, *Int. J. Nanomed.*, 2013, **8**, 1897–1906.
- 25 M. Faraday, *Philos. Trans. R. Soc. London*, 1857, **147**, 145–181.
- 26 P. K. Jain, K. S. Lee, I. H. El-Sayed and M. A. El-Sayed, *J. Phys. Chem. B*, 2006, **110**, 7238–7248.
- 27 C. Greulich, J. Diendorf, J. Gessmann, T. Simon, T. Habijan, G. Eggeler, T. A. Schildhauer, M. Epple and M. Koller, *Acta Biomater.*, 2011, **7**, 3505–3514.
- 28 C. Greulich, J. Diendorf, T. Simon, G. Eggeler, M. Epple and M. Koller, *Acta Biomater.*, 2011, **7**, 347–354.
- 29 A. M. Scherbarth, J. Langer, A. Bushmelev, D. van Berlo, P. Haberzettl, F. J. van Schooten, A. M. Schmidt, C. R. Rose, R. P. Schins and C. Albrecht, *Part. Fibre Toxicol.*, 2011, **8**, 31.
- 30 B. Schmidt, K. Loeschner, N. Hadrup, A. Mortensen, J. J. Sloth, C. B. Koch and E. H. Larsen, *Anal. Chem.*, 2011, **83**, 2461–2468.
- 31 B. D. Chithrani, A. A. Ghazani and W. C. Chan, *Nano Lett.*, 2006, **6**, 662–668.
- 32 K. Loeschner, M. S. Brabrand, J. J. Sloth and E. H. Larsen, *Anal. Bioanal. Chem.*, 2014, **406**, 3845–3851.
- 33 F. Laborda, E. Bolea and J. Jimenez-Lamana, *Anal. Chem.*, 2014, **86**, 2270–2278.
- 34 J. T. Fourie, *Gold Bull.*, 1982, **15**, 2–6.
- 35 L. Mikkelsen, K. A. Jensen, I. K. Koponen, A. T. Saber, H. Wallin, S. Loft, U. Vogel and P. Moller, *Nanotoxicology*, 2013, **7**, 117–134.
- 36 J. A. Heymann, D. Shi, S. Kim, D. Bliss, J. L. Milne and S. Subramaniam, *J. Struct. Biol.*, 2009, **166**, 1–7.
- 37 C. P. Garcia, V. Sumbayev, D. Gilliland, I. M. Yasinska, B. F. Gibbs, D. Mehn, L. Calzolari and F. Rossi, *Sci. Rep.*, 2013, DOI: 10.1038/srep01326, 1326.
- 38 V. Lulevich, Y. P. Shih, S. H. Lo and G. Y. Liu, *J. Phys. Chem. B*, 2009, **113**, 6511–6519.
- 39 M. Poot, T. J. Kavanagh, H. C. Kang, R. P. Haugland and P. S. Rabinovitch, *Cytometry*, 1991, **12**, 184–187.
- 40 J. Sebastia, R. Cristofol, M. Martin, E. Rodriguez-Farre and C. Sanfeliu, *Cytometry, Part A*, 2003, **51**, 16–25.
- 41 D. Vercauteren, R. E. Vandenbroucke, A. T. Jones, J. Rejman, J. Demeester, S. C. De Smedt, N. N. Sanders and K. Braeckmans, *Mol. Ther.*, 2010, **18**, 561–569.
- 42 H. Damke, T. Baba, A. M. van der Blik and S. L. Schmid, *J. Cell Biol.*, 1995, **131**, 69–80.
- 43 E. Elias and J. Boyer, *Science*, 1979, **206**, 1404–1406.
- 44 T. Ogiso, M. Iwaki and K. Mori, *Biochim. Biophys. Acta*, 1981, **649**, 325–335.
- 45 G. P. Otto and B. J. Nichols, *J. Cell Sci.*, 2011, **124**, 3933–3940.
- 46 B. D. Chithrani and W. C. Chan, *Nano Lett.*, 2007, **7**, 1542–1550.
- 47 W. Jiang, B. Y. Kim, J. T. Rutka and W. C. Chan, *Nat. Nanotechnol.*, 2008, **3**, 145–150.
- 48 C. D. Walkey, J. B. Olsen, H. Guo, A. Emili and W. C. Chan, *J. Am. Chem. Soc.*, 2012, **134**, 2139–2147.
- 49 S. H. Brewer, W. R. Glomm, M. C. Johnson, M. K. Knag and S. Franzen, *Langmuir*, 2005, **21**, 9303–9307.
- 50 I. S. Hueck, H. G. Hollweg, G. W. Schmid-Schonbein and G. M. Artmann, *Am. J. Physiol.: Cell Physiol.*, 2000, **278**, C873–C878.
- 51 E. C. Cho, Q. Zhang and Y. Xia, *Nat. Nanotechnol.*, 2011, **6**, 385–391.
- 52 J. M. Cohen, J. G. Teeguarden and P. Demokritou, *Part. Fibre Toxicol.*, 2014, **11**, 20.
- 53 P. Hinderliter, K. Minard, G. Orr, W. Chrisler, B. Thrall, J. Pounds and J. Teeguarden, *Part. Fibre Toxicol.*, 2010, **7**, 36.
- 54 G. DeLoid, J. M. Cohen, T. Darrach, R. Derk, L. Rojasasakul, G. Pyrgiotakis, W. Wohlleben and P. Demokritou, *Nat. Commun.*, 2014, **5**, 3514.
- 55 R. M. Bohmer and N. J. King, *Cytometry*, 1984, **5**, 543–546.
- 56 H. Suzuki, T. Toyooka and Y. Ibuki, *Environ. Sci. Technol.*, 2007, **41**, 3018–3024.

- 57 R. M. Zucker, K. M. Daniel, E. J. Massaro, S. J. Karafas, L. L. Degn and W. K. Boyes, *Cytometry, Part A*, 2013, **83**, 962–972.
- 58 R. M. Zucker, E. J. Massaro, K. M. Sanders, L. L. Degn and W. K. Boyes, *Cytometry, Part A*, 2010, **77**, 677–685.
- 59 E. E. Connor, J. Mwamuka, A. Gole, C. J. Murphy and M. D. Wyatt, *Small*, 2005, **1**, 325–327.
- 60 H. T. McMahon and E. Boucrot, *Nat. Rev. Mol. Cell Biol.*, 2011, **12**, 517–533.
- 61 H. H. Li, J. Li, K. J. Wasserloos, C. Wallace, M. G. Sullivan, P. M. Bauer, D. B. Stolz, J. S. Lee, S. C. Watkins, C. M. St Croix, B. R. Pitt and L. M. Zhang, *PLoS One*, 2013, **8**, e81903.
- 62 J. Kneipp, H. Kneipp, M. McLaughlin, D. Brown and K. Kneipp, *Nano Lett.*, 2006, **6**, 2225–2231.
- 63 Q. Zhang, V. M. Hitchins, A. M. Schrand, S. M. Hussain and P. L. Goering, *Nanotoxicology*, 2011, **5**, 284–295.
- 64 A. M. Alkilany and C. J. Murphy, *J. Nanopart. Res.*, 2010, **12**, 2313–2333.
- 65 N. R. Jacobsen, A. T. Saber, P. White, P. Moller, G. Pojana, U. Vogel, S. Loft, J. Gingerich, L. Soper, G. R. Douglas and H. Wallin, *Environ. Mol. Mutagen*, 2007, **48**, 451–461.
- 66 N. R. Jacobsen, P. Moller, C. A. Cohn, S. Loft, U. Vogel and H. Wallin, *Mutat. Res.*, 2008, **641**, 54–57.
- 67 N. R. Jacobsen, P. A. White, J. Gingerich, P. Moller, A. T. Saber, G. R. Douglas, U. Vogel and H. Wallin, *Environ. Mol. Mutagen*, 2011, **52**, 331–337.
- 68 L. K. Vesterdal, L. Mikkelsen, J. K. Folkmann, M. Sheykhzade, Y. Cao, M. Roursgaard, S. Loft and P. Moller, *Toxicol. Lett.*, 2012, **214**, 19–26.